

Description of the plasma delay effect in silicon detectors

Z. Sosin

October 30, 2018

Institute of Physics, Jagellonian University

Abstract

A new method of modeling of the current signal induced by charged particle in silicon detectors is presented. The approach is based on the Ramo-Shockley theorem for which the charge carrier velocities are determined by taking into account not only the external electric field generated by the electrodes, but also the Coulomb interaction between the electron and hole clouds as well as their diffusion.

keywords:

Plasma delay
Current pulse
Pulse shape analysis
Particles identification
Silicon detector

1 Introduction

It is obvious that identification of particles and fragments produced in nuclear reactions is crucial for any experimental or technical work in nuclear physics. Among different ways of identifying charged particles the classical $\Delta E - E$ telescope method remains still the flagship. Recently, an alternative method based on the Pulse Shape Discrimination (PSD) technique applied for silicon

detectors is being developed and is increasingly drawing attention. Recent results demonstrate that the method can offer charge and isotopic identification comparable to that obtained with the classical $\Delta E - E$ method. The main advantage of the PSD method comes from the fact that it requires only one electronic channel for detection and identification. It is thus an important point for designing and constructing multi-detector systems.

A significant difference between the $\Delta E - E$ and the PSD techniques results from the fact that the former is governed basically by the energy loss process (Bragg curve), while the latter is primarily related to the Plasma Delay Effect (PDE) [1-6]. In silicon detectors, this effect manifests itself with shortening of the pulse rise time with decreasing Z for low and intermediate mass fragments, for which the generated charge is practically completely collected by the detector electrodes. The experimental data demonstrates that the PDE concerns particles with small Z , for which the Pulse Height Defect (PHD) is still of little importance.

For better understanding of the identification idea associated with PSD technique, and for its future development, it is crucial to have at ones command a perfect simulation of the time dependence of the experimental signal produced by an ion with a given charge, Z , atomic mass, A , and energy, E . The main goal of such a simulation is to describe the extraction and collection of the generated charge carriers moving in the external electric field distorted due to the presence of a highly ionized track and due to the diffusion process of the carriers.

As presented in [7], an approach in which the distortion of the electric field caused by the generated carriers is neglected, is able to correctly describe the current signals for light charged particles (LCP), e.g. protons. However, this simplified approach completely fails in case of heavy ions (HI) for which the collection time of the generated carriers gets longer ($\tau^{HI} > \tau^{LCP}$). Historically, this difference, associated to a slower carrier collection for HI, was quantified as a plasma delay (PD) effect. Since this effect influences the current signal rise-time, it appears to be crucial for the PSD technique.

An attempt to describe phenomenologically the delayed carrier collection time in silicon detectors has been recently proposed in [8]. The proposed description took into account the polarization of the electron-hole pairs generated by the HI and connected it to the relative dielectric permittivity. Another important assumption was that the dissociation of pairs in time occurred with a constant probability and the modified electric field, inside and outside of the ion range, was given by the Maxwell equation for the electric

field in the inhomogeneous medium. With these assumptions, the model was indeed able to describe the experimental pulse shapes quite accurately.

In the present paper we propose another, more microscopic approach. The main model assumptions are the following:

- i. Propagation of the electric charges (electrons, holes) generated in the detector is represented by evolution of the Gaussian clouds for which the centroids and variances are treated as independent variables.
- ii. Position of the centroid of each Gaussian is governed by the drift process, while its variance undergoes both, diffusion and the drift process.

The first results of the model calculations indicate some binding effects between the holes and electrons, in a region similar to that predicted by the phenomenological model of Ref. [8]. In this region also the electric field shows similar behavior to that presented in [8].

The detailed description of the new model is presented in the following section. The preliminary results of the calculations and comparison to the experimental data are presented in Section 3; Conclusions and possible extensions of the model applicability are given in Section 4.

2 Description of the model

A particle entering the silicon detector is assumed to degrade its energy according to the Bragg curve which relates the generated ionization $B(x)$ to the particle position x . We assume that the X direction is perpendicular to the detector surface. In order to describe the initial, local, density of the electrons $\rho_e(\mathbf{r}, t = 0)$ and holes $\rho_h(\mathbf{r}, t = 0)$ we assume that the ionization is proportional to the local stopping power $B(x) = \frac{1}{w} \frac{dE}{dx}(x)$, where $w = 3.62$ eV is the energy for an electron-hole pair production and $\frac{dE}{dx}(x)$ is the local stopping power [9]. Just after stopping of the impinging ion, the carrier density can be described as:

$$\rho_e(\mathbf{r}, t = 0) = -\rho_h(\mathbf{r}, t = 0) = - \int B(x') \delta(x - x') \delta(y) \delta(z) dx' \quad (1)$$

where $\mathbf{r} = [x, y, z]$. This assumption states that for $t = 0$ the ionization is localized along the X axis only and disappears elsewhere.

In order to describe the time evolution of the generated ionization we assume its distribution in the following form:

$$\rho_e(\mathbf{r}, t) = \int B_e(x', t) G_e(x - x', y, z, t) dx' \quad (2)$$

$$\rho_h(\mathbf{r}, t) = \int B_h(x', t) G_h(x - x', y, z, t) dx' \quad (3)$$

which is analog to (1) and we set:

$$- B_e(x, t = 0) = B_h(x, t = 0) = B(x) \quad (4)$$

Functions G_e and G_h are assumed to be Gaussians:

$$G_e(x - x', y, z, t) = \frac{1}{\sqrt{(2\pi)^3 \sigma_e^3(x, t)}} \exp\left(-\frac{(x - x')^2 + y^2 + z^2}{2\sigma_e^2(x, t)}\right) \quad (5)$$

and

$$G_h(x - x', y, z, t) = \frac{1}{\sqrt{(2\pi)^3 \sigma_h^3(x, t)}} \exp\left(-\frac{(x - x')^2 + y^2 + z^2}{2\sigma_h^2(x, t)}\right) \quad (6)$$

If $\sigma_e \rightarrow 0$ and $\sigma_h \rightarrow 0$ for $t \rightarrow 0$ then the functions G_e and G_h can be regarded as representations of the δ function, thus:

$$G_e(x - x', y, z, t = 0) = G_h(x - x', y, z, t = 0) = \delta(x - x')\delta(y)\delta(z) dx \quad (7)$$

Now, the goal is to describe the time evolution of the functions B_e , B_h and G_e , G_h (for determination of G_e , G_h it is sufficient to derive the time evolution of their variances σ_e^2 and σ_h^2). In order to do it we define the one dimensional densities associated with the variable x as:

$$\eta_e(x, t) = \int_{-\infty}^{\infty} dy \int_{-\infty}^{\infty} dz \rho_e(\mathbf{r}, t) \quad (8)$$

$$\eta_h(x, t) = \int_{-\infty}^{\infty} dy \int_{-\infty}^{\infty} dz \rho_h(\mathbf{r}, t) \quad (9)$$

and we divide the thickness of the detector d_{S_i} into N intervals $\Delta x = \frac{d_{S_i}}{N}$. Let us assume that in the interval Δx_i ($i = 1, N$) the associated values of σ_{ei} and σ_{hi} do not change substantially within the radius of a few sigma around Δx_i , and that a linear approximation can be used for the functions $B_e(x', t)$ and $B_h(x', t)$ within Δx_i :

$$B_e(x', t) = p_{ei}(t)x' + q_{ei}(t) \quad (10)$$

$$B_h(x', t) = p_{hi}(t)x' + q_{hi}(t) \quad (11)$$

With the above assumption for x within an interval Δx_i one can approximate the densities:

$$\eta_e(x, t) \simeq \int_{-\infty}^{\infty} dx' \int_{-\infty}^{\infty} dy \int_{-\infty}^{\infty} dz (p_{ei}(t)x' + q_{ei}(t)) G_e(x-x', y, z, t) = p_{ei}(t)x + q_{ei}(t) \quad (12)$$

$$\eta_h(x, t) \simeq \int_{-\infty}^{\infty} dx' \int_{-\infty}^{\infty} dy \int_{-\infty}^{\infty} dz (p_{hi}(t)x' + q_{hi}(t)) G_h(x-x', y, z, t) = p_{hi}(t)x + q_{hi}(t) \quad (13)$$

which means that, in practice, one can use the same coefficients for linear expansion of both, the densities η_e , η_h and of the functions B_e , B_h .

We introduce also the $x_{e0}(t)$ and $x_{eN}(t)$ coordinates, which denote the beginning and end of the $B_e(x, t)$ distributions for electrons. Similar coordinates $x_{h0}(t)$ and $x_{hN}(t)$ are introduced for holes (see right-upper panel on Fig. 2).

2.1 Electric field determination

In order to determine the drift velocity associated with the centers of Gaussians G_e , G_h we have to calculate the respective effective electric field acting on the carriers described by above distributions. Such a field is determined by a static voltage applied to the detector electrodes and by the Coulomb interaction between the Gaussian charge clouds. The detector static field at position x , considered from the rear side of the detector (order $n - p$ from

the point of view of the particle entering the detector, see e.g. [8]), is given as:

$$E_{stat}(x) = \frac{2V_d x}{d_{Si}^2} + \frac{V - V_d}{d_{Si}} \quad (14)$$

where the bias voltage V is assumed to be higher than the depletion voltage V_d which for the bulk concentration of donors N_D and permittivity $\varepsilon = \varepsilon_r \varepsilon_0$ reads as:

$$V_d = \frac{eN_D d^2}{2\varepsilon_r \varepsilon_0} \quad (15)$$

In order to find the modification of the electric field caused by the generated plasma, let us consider two Gaussians describing the distribution of the charges Z_1 , Z_2 , centered at a relative distance $r_{12} = |\mathbf{r}_1 - \mathbf{r}_2|$ and characterized by variances σ_1^2 , σ_2^2 respectively. The mutual interaction potential of the clouds can then be expressed in the form which can be often found in quantum molecular dynamics calculations (see e.g. [10])

$$\begin{aligned} v(r_{01}, r_{02}, \sigma_1, \sigma_2) &= \frac{e^2 Z_1 Z_2}{(2\pi\sigma_1\sigma_2)^3} \iint \frac{\exp\left(\frac{-(\mathbf{r}_1 - \mathbf{r}_{01})^2}{2\sigma_1^2}\right) \exp\left(\frac{-(\mathbf{r}_2 - \mathbf{r}_{02})^2}{2\sigma_2^2}\right)}{|\mathbf{r}_1 - \mathbf{r}_2|} d^3\mathbf{r}_1 d^3\mathbf{r}_2 = \\ &= e^2 Z_1 Z_2 \frac{\operatorname{erf}\left(\frac{r_{12}}{\sqrt{2}\sigma}\right)}{r_{12}} \end{aligned} \quad (16)$$

where $\sigma = \sqrt{\sigma_1^2 + \sigma_2^2}$.

Let us now assume that the intervals Δx_i are small enough to enable the linear approximation for the charge densities ρ_e , ρ_h and the functions B_e , B_h with the use of the coefficients p and q . For simplicity, we introduce variables p , q in lieu of the $p_{ei}(t)$, $p_{hi}(t)$ and $q_{ei}(t)$, $q_{hi}(t)$. If we denote the endpoints of the Δx_i interval by c and d then for a Gaussian centered at a point a and representing the charge Z_a , its interaction with the charge located in the interval $\Delta x_i = (c, d)$ given by (12) and (13), can be formulated as:

$$V_C(a, c, d, p, q, \sigma_a, \sigma_i) = \frac{e^2}{\varepsilon} Z_a \int_c^d dx (px + q) \frac{\operatorname{erf}\left(\frac{|x-a|}{\sqrt{2}\sigma_s}\right)}{|x-a|} \quad (17)$$

where the σ_a and σ_i above denote the standard deviations of the Gaussian describing the charge Z_a and of the Gaussian from the interval Δx_i , respectively, and $\sigma_s = \sqrt{\sigma_a^2 + \sigma_i^2}$.

The above form allows us to describe the respective effective electric field E_x acting on the Gaussian located at a point a as

$$E_x(a, c, d, p, q, \sigma_a, \sigma_i) = -\frac{1}{Z_a} \frac{\partial V_C}{\partial a} = -\frac{e^2}{\varepsilon} \int_c^d dx (px + q) \frac{\partial}{\partial a} \frac{\operatorname{erf}\left(\frac{|x-a|}{\sqrt{2}\sigma_s}\right)}{|x-a|} \quad (18)$$

Since $\frac{\partial}{\partial a} = -\frac{\partial}{\partial x}$, the above formula can be expressed as:

$$\begin{aligned} E_x(a, c, d, p, q, \sigma_a, \sigma_i) &= \frac{e^2}{\varepsilon} \int_c^d dx (px + q) \frac{\partial}{\partial x} \frac{\operatorname{erf}\left(\frac{|x-a|}{\sqrt{2}\sigma_s}\right)}{|x-a|} = \\ &= \frac{e^2}{\varepsilon} q \left(\frac{\operatorname{erf}\left(\frac{|d-a|}{\sqrt{2}\sigma_s}\right)}{|d-a|} - \frac{\operatorname{erf}\left(\frac{|c-a|}{\sqrt{2}\sigma_s}\right)}{|c-a|} \right) + \frac{e^2}{\varepsilon} p \int_c^d dx x \frac{\partial}{\partial x} \frac{\operatorname{erf}\left(\frac{|x-a|}{\sqrt{2}\sigma_s}\right)}{|x-a|} \end{aligned} \quad (19)$$

After integrating by parts one obtains:

$$\begin{aligned} E_x &= \frac{e^2}{\varepsilon} q \left(\frac{\operatorname{erf}\left(\frac{|d-a|}{\sqrt{2}\sigma_s}\right)}{|d-a|} - \frac{\operatorname{erf}\left(\frac{|c-a|}{\sqrt{2}\sigma_s}\right)}{|c-a|} \right) + \frac{e^2}{\varepsilon} p \left(d \frac{\operatorname{erf}\left(\frac{|d-a|}{\sqrt{2}\sigma_s}\right)}{|d-a|} - c \frac{\operatorname{erf}\left(\frac{|c-a|}{\sqrt{2}\sigma_s}\right)}{|c-a|} \right) + \\ &\quad - \frac{e^2}{\varepsilon} p \int_c^d dx \frac{\operatorname{erf}\left(\frac{|x-a|}{\sqrt{2}\sigma_s}\right)}{|x-a|} \end{aligned} \quad (20)$$

The last integral can be easily evaluated by expanding the error function.

The total effective electric field modified due to the presence of plasma can be obtained by summing up contributions of charges located in all intervals (c_i, d_i) and of their mirror charges induced in the detector electrodes (see Fig. 1).

In order to determine the time evolution of the charge distribution one has to know, in addition, the generalized force associated with the σ_a variable. Similarly as for the effective electric field, the net value of the force acting in the σ_a direction can be obtained by summing over all ingredients associated with the charge distribution. This leads to the following expression for the interaction with the charge located in the Δx_i interval:

$$F_{\sigma_a, a, cd} = -\frac{\partial V_C}{\partial \sigma_a} = -\frac{e^2}{\varepsilon} Z_a \int_c^d dx (px + q) \frac{\partial}{\partial \sigma_a} \frac{\operatorname{erf}\left(\frac{|x-a|}{\sqrt{2}\sigma_s}\right)}{|x-a|} =$$

$$\begin{aligned}
&= -Z_a \frac{e^2 p \sigma_a}{\sqrt{\frac{\pi}{2}} \varepsilon \sigma_s} \left(\exp \left(-\frac{(a-d)^2}{2\sigma_s^2} \right) - \exp \left(-\frac{(a-c)^2}{2\sigma_s^2} \right) \right) + \\
&\quad + Z_a \frac{e^2 \sigma_a (ap + q)}{\varepsilon \sigma_s^2} \left(\operatorname{erf} \left(\frac{(a-d)}{\sqrt{2}\sigma_s} \right) - \operatorname{erf} \left(\frac{(a-c)}{\sqrt{2}\sigma_s} \right) \right) \quad (21)
\end{aligned}$$

Now we are in position to calculate the time evolution of the charge generated in the detector. This process is determined by the drift and by the diffusion of the interacting clouds of electrons and holes. We will consider the evolution of the centroids and of the variances of Gaussians representing a fraction of the charge distribution located in the middle of the intervals Δx_i and at the start- and end-points of the distributions of electrons and holes (points $x_{e0}(t)$, $x_{eN}(t)$ and $x_{h0}(t)$, $x_{hN}(t)$).

2.2 Evolution of the function B

In the present subsection we will describe the numerical method used to determine the time evolution of the ionization clouds. In the following we assume that the evolution of the functions B_e , B_h is determined by the time evolutions of the coefficients p_{ei} , q_{ei} and p_{hi} , q_{hi} . In order to find how the expansion coefficients p_{ei} , q_{ei} and p_{hi} , q_{hi} propagate in time, we have to investigate the time evolution of the functions $\eta_e(x, t)$ and $\eta_h(x, t)$.

Below we consider the formulas for electrons only, keeping in mind that the formulas for holes are analogical.

As we will show later

$$\frac{\partial}{\partial t} \eta_e(x, t) = -\frac{\partial}{\partial x} (\eta_e(x, t) v_{xe}(x, t)) \quad (22)$$

thus, the differential $d\eta_e(x, t)$ can be written as

$$d\eta_e(x, t) = - \left(v_{xei}(x, t) \frac{\partial}{\partial x} \eta_e(x, t) + \eta_e(x, t) \frac{\partial}{\partial x} v_{xe}(x, t) \right) dt \quad (23)$$

If the x_i denotes the center of the interval Δx_i and q_{ei} and p_{ei} are the coefficients of linear expansion

$$\eta_e(x, t) = p_{ei}(t)(x - x_i) + q_{ei} \quad (24)$$

and, if one denotes the average velocity and the average linear density associated with the interval Δx_i by $v_{x_{ei}}(t)$ and $\eta_{x_{ei}}(t)$, respectively, then:

$$d\eta_{ei}(t) = - (v_{x_{ei}}(t)p_{ei}(t) + \eta_{ei}(t)\varphi_{x_{ei}}(t)) dt \quad (25)$$

Here, $\varphi_{x_{ei}}(t)$ is the differential coefficient of $v_{x_{ei}}(x, t)$ at the point x_i . As one can see, in order to calculate the above increment, we have to trace the time dependent tables of $\eta_{ei}(t)$, $v_{x_{ei}}(t)$. The tables of $p_{ei}(t)$, $q_{ei}(t)$ and $\varphi_{x_{ei}}(t)$ are obtained by fitting the smooth curves to the distributions $\eta_{ei}(t)$, $v_{x_{ei}}(t)$ in every time step. For $t = 0$ the $\eta_{ei}(t = 0)$ is given by the Bragg curve. In order to make use of the formula (25) we need to construct the respective tables for velocities. Knowing the effective electric field for electrons in the x direction, $E_{x_{ei}}$, one can assume that the respective average velocity of the center of Gaussian located at a point x_i is proportional to the strength of the field:

$$v_{x_{ei}} = \mu_{xe} E_{x_{ei}} \quad (26)$$

where μ_{xe} and μ_{xh} are the electron and hole mobilities, respectively.

Knowing the drift velocity, one can calculate the evolution of the charge deposited in every interval Δx_i including the edge intervals with variable ends $x_{e0}(t)$, $x_{eN}(t)$ and $x_{h0}(t)$, $x_{hN}(t)$.

2.3 Charge propagation in the perpendicular direction

The diffusion and transport processes in the electric field influence also the widths of the charge distributions located in every Δx_i interval. Extending the above reasoning we can assume that the velocity, $v_{\sigma_{ei}}$, describing the rate of the standard deviation expansion in perpendicular direction has three components:

$$v_{\sigma_{ei}} = v_{\sigma_{ei}}^E + v_{\sigma_{ei}}^D + v_{\sigma_{ei}}^T \quad (27)$$

The first term, $v_{\sigma_{ei}}^E$, results from the field described by (21). In analogy to the charge drift in x direction, one can assume that this component is proportional to the field acting on the charge Z_a associated with the Gaussian with a standard deviation σ_a

$$E_{\sigma_{ei}} = \frac{F_{\sigma_a}}{Z_a} \quad (28)$$

where F_{σ_a} is the net force given by interaction (21). Thus, the respective velocity can be expressed as

$$v_{\sigma_{ei}}^E = \mu_{\sigma_e} E_{\sigma_{ei}} \quad (29)$$

where, the μ_{σ_e} parameter is the only free parameter of the model. It seems, however, that it can be determined theoretically in the future. A similar parameter for description of the hole propagation can be calculated assuming the following proportion:

$$\frac{\mu_{\sigma_e}}{\mu_{\sigma_h}} = \frac{\mu_{xe}}{\mu_{xh}} \quad (30)$$

The velocity $v_{\sigma_{ei}}^D$ follows from the solution of the second Fick's law for diffusions of Gaussian density distributions:

$$v_{\sigma_{ei}}^D = \frac{\partial \sigma_{ei}}{\partial t} \Big|_{v_{\sigma_{ei}}^E=0, v_{\sigma_{ei}}^T=0} = \frac{D_e}{\sigma_{ei}} \quad (31)$$

where D_e is the diffusion coefficient for electrons.

Another process which affects, on average, the widths of the respective Gaussian distributions used to describe the charge located in the interval Δx_i , is related to the transport of the carriers. In order to describe this process we consider an increase of the variance, σ^2 , of the Gaussian distribution of the charge of Z particles contained in an interval Δx , with linear density $\eta(x) = \frac{Z}{\Delta x}$. Let the $\sum r_i^2$ denote the sum of squares of deviations of particle positions from the average. In this consideration we neglect the influence of the diffusion and of mutual interactions of clouds on the propagation of the variance.

The change of $\sigma^2 \equiv \frac{\sum r_i^2}{Z}$, resulting from the flow of particles into and out of the cell Δx (with the net value of dZ) is, in general, equal to

$$d\sigma^2 = \frac{d(\sum r_i^2)}{Z} - \frac{\sigma^2(x)dZ}{Z} \quad (32)$$

As one can see, in order to find the increment $d\sigma^2$ we have to find the increments dZ and $d(\sum r_i^2)$.

Let us begin with the description of $d(\sum r_i^2)$. If the accretion of particles in an interval Δx across the points $x_1 = x - \Delta x/2$ and $x_2 = x + \Delta x/2$ is denoted by dZ_1 and dZ_2 , respectively, and the variances at these points are

denoted by $\sigma_1^2 = \sigma^2(x - \Delta x/2)$ and $\sigma_2^2 = \sigma^2(x + \Delta x/2)$, respectively, then the increment of the sum $\sum r_i^2$ can be determined as:

$$d\left(\sum r_i^2\right) = \sigma_1^2 dZ_1 - \sigma_2^2 dZ_1 \quad (33)$$

Denoting the velocities of particles at points x_1 and x_2 by $v(x - \Delta x/2)$ and $v(x + \Delta x/2)$, respectively, the accretions dZ_1 and dZ_2 can be determined as

$$dZ_1 = \eta(x - \Delta x/2) v(x - \Delta x/2) dt \quad (34)$$

$$dZ_2 = \eta(x + \Delta x/2) v(x + \Delta x/2) dt \quad (35)$$

Now one can calculate the increment $d\left(\sum r_i^2\right)$ as

$$d\left(\sum r_i^2\right) = -dt \cdot \Delta x \cdot$$

$$\cdot \left[\frac{\sigma^2(x + \Delta x/2) \eta(x + \Delta x/2) v(x + \Delta x/2) - \sigma^2(x - \Delta x/2) \eta(x - \Delta x/2) v(x - \Delta x/2)}{\Delta x} \right] \quad (36)$$

The expression in square brackets tends to the partial derivate $\frac{\partial(\sigma^2(x)\eta(x)v(x))}{\partial x}$ for $\Delta x \rightarrow 0$.

Similarly, the increment $dZ = dZ_1 - dZ_2$ can be written as

$$dZ = -\Delta x \left[\frac{\eta(x + \Delta x/2) v(x + \Delta x/2) - \eta(x - \Delta x/2) v(x - \Delta x/2)}{\Delta x} \right] dt \quad (37)$$

and again, in the limit of $\Delta x \rightarrow 0$ the expression in square brackets approaches to $\frac{\partial(\eta(x)v(x))}{\partial x}$, which has already been used in (22).

Taking the above into account, setting $Z = \eta(x)\Delta x$ and taking the $\Delta x \rightarrow 0$ limit, eq. (32) can be transformed into:

$$d\sigma^2(x) = \left[\frac{-\partial(\sigma^2(x)\eta(x)v(x))}{\partial x} + \frac{\sigma^2(x)\partial(\eta(x)v(x))}{\partial x} \right] \frac{dt}{\eta(x)} = \frac{-v(x)\partial(\sigma^2(x))}{\partial x} dt \quad (38)$$

what gives

$$\frac{\partial \sigma^2}{\partial t} = -v \frac{\partial \sigma^2}{\partial x} \Rightarrow \frac{\partial \sigma}{\partial t} = -v \frac{\partial \sigma}{\partial x} \quad (39)$$

Finally for $v_{\sigma_{ei}}^E = 0$ and $v_{\sigma_{ei}}^D = 0$ one can write

$$v_{\sigma_{ei}}^T = \left. \frac{\partial \sigma_{ei}}{\partial t} \right|_{v_{\sigma_{ei}}^E=0, v_{\sigma_{ei}}^D=0} = -v_{x_{ei}} \frac{\partial \sigma_{ei}}{\partial x} \quad (40)$$

In order to use the above formula we trace the changes of the vector of σ_{ei} values as a function of the position index, i . Knowledge of velocities $v_{\sigma_{ei}}^E$, $v_{\sigma_{ei}}^D$ and $v_{\sigma_{ei}}^T$ allows to calculate the propagation of the width of the distribution of electrons. The formulas for holes are analogical.

3 First prediction of the model and comparison with the experimental data

For the first comparison of the model prediction with the experimental data we choose the data for ^{12}C ion which have already been used in [8]. This gives also the opportunity to compare the present model predictions with those obtained in a more phenomenological approach. For the measurement the neutron transmutation doped (n-TD) silicon detector [11] was used. This n-type bulk and extremely thin p-type zone has a thickness $d_{Si} = 310 \mu\text{m}$. The energy measurement was performed using the charge output, while the current pulses were measured using the current output of the same preamplifier, described in [7]. This paper presents also in detail the experimental setup and conditions used for the ^{12}C ions (and LCP).

Before describing the induced current pulse, we focus first on the propagation of the electric field and the propagation of the electron and hole densities in parallel and perpendicular directions. The evolution of these observables is important for understanding the mechanism of the plasma delay process. In the following, we consider an ^{12}C ion impinging on the n-type rear side of the silicon detector. This, so called “rear-mount”, gives quite different shapes as compared to the “standard mount”, and these pulse shapes are much better suited for the PSD technique [7].

For actual calculations it is necessary to set some physical coefficients describing the electric field propagation, as well as coefficients describing the drift and diffusion process in silicon. In table 1 we collect values of these

parameters:

feature	symbol	value	remarks
energy per e-h pair creation	w	3.6 $\frac{eV}{pair}$	material constant
silicon dielectric, permittivity	ϵ_r	11.7	material constant
electrons mobility	μ_{xe}	135 $\frac{\mu m^2}{Vns}$	material constant
holes mobility	μ_{xh}	47.5 $\frac{\mu m^2}{Vns}$	material constant
electrons variance mobility	$\mu_{\sigma e}$	2 $\frac{\mu m^2}{Vns}$	free parameter
holes variance mobility	$\mu_{\sigma h}$	$\mu_{\sigma h} = \mu_{\sigma e} \frac{\mu_{xh}}{\mu_{xe}}$	model assumption
diffusion coefficient for electrons	D_e	3.49 $\frac{\mu m^2}{ns}$	material constant
diffusion coefficient for holes	D_h	1.228 $\frac{\mu m^2}{ns}$	material constant

As already mentioned, the electric field propagation results from the static detector bias and from the generated charge density propagation. At the starting point, when the generated electrons and holes are almost exactly at the same positions, the electric field is still equal to the external one (14). This field, for $t=0$, is denoted in Fig. 2 by a dotted line. After this initial moment the static field causes the shift of the electron and hole distributions and therefore in the next moment some of the carriers are moved outside of the overlap region. Next, the variance of the Gaussian partial density distribution associated with these carriers begins to grow, due to the non-compensated electric field in perpendicular direction. This effect, which is displayed in Fig. 3, causes breaking of the initial bonds between the electrons and holes. As a result, the considered electrons and holes start leaking slowly from the overlap region and begin moving in opposite directions. At the same time, the increasing shift between electrons and holes leads to significant reduction of the electric field in the interaction region. This scenario is well associated with the postulates of the phenomenological model of ref. [8].

The evolution of the charge density, the effective electric field and the variances of the Gaussian partial densities are presented in Figs 2-5 in which the blue lines represent the dependences for the electrons while the red ones represent the holes. Fig. 2 shows the evolution of the linear electron and hole densities. One can see that, during the first 20-30 ns, the electrons and holes

remain bound in the region close to the detector surface. After that time, one can observe the electric field restitution practically in the whole detector area. The time behavior of the electric field is presented in Fig. 3. In order to save the calculation time, the field is calculated only at points where the density of the particles is not equal to zero. Fig. 4 presents the evolution of the width of the charge distributions. We can notice that in the overlap region the effective electric field is reduced to very low value. As one can see, the evolutions of the electric field and of the charge densities (in parallel and perpendicular directions) are strongly correlated.

Up to now, the mutual Coulomb interactions between the charge clouds have been taken into account. In order to see the importance of these mutual interactions, they have been neglected in the charge density evolutions presented in Fig 5. As one can see, in this case, the collection time becomes about three times shorter, due to the lack of binding between the electrons and holes. Knowledge of the charge propagation, by using of the Ramo-Shockley theorem [12, 13, 14], allowed as to determine the current pulse time dependence.

In order to obtain a rough estimate of the pulse shape, we describe the partial current associated with the Gaussian cloud in approximate way. For simplification, using Ramo-Shockley theorem, we replace the Gaussian charge distribution by a point-like one. Such an approach neglects effects associated with the charge diffuseness, particularly for clouds moving closely to the detector electrodes.

The result of such a calculation is presented in fig 6. The total current pulse is denoted by black solid line while the electron and hole contributions are represented by the blue and red ones, respectively.

For comparison of the calculated pulse with the experimental one the primary pulses from Fig. 6. have been corrected (see [3]) for the preamplifier's response. The results are shown in Fig. 7. We have to stress that in the present calculations we did not search for the best value of the $\mu_{\sigma e}$ parameter. We also did not consider some quite complicated factors, specified below, which could affect the obtained results and which will be a subject of the forthcoming paper:

- i) precision of the Energy-Range tables (average accuracy of about 10%, see [9]),
- ii) diffuseness of the Gaussian clouds and its presence in the application of the Ramo-Shockley theorem,
- iii) dead layers of the detector and their effect on the measured energy (as

one can see on Fig. 8, for 80 MeV ^{12}C the collection time is very sensitive on the ion energy),

iv) accuracy of the active detector thickness and of the electric field determination,

v) accuracy of the preamplifier response description.

In order to demonstrate that the present model is able to describe correctly the plasma delay effect, in Fig. 8 we present the correlation between the collection time and the energy loss for ^{10}B , ^{12}C , and ^{14}N ions. We use the collection time rather than the experimentally preferred rise time, noting that these two observables are strongly correlated. Fig. 8 shows that the model can reproduce the experimental trends, especially the characteristic “back-bending” of identification curves at low energies.

4 Conclusions

We have proposed a description of the evolution of charge density and of the effective electric field by taking into account the mutual Coulomb interactions between the charge carrier distributions. According to the present approach the plasma delay effect is associated with the propagation of the carriers in both directions, perpendicular and parallel to the primary ionization path.

The duration of the obtained pulse for the 80 MeV ^{12}C ion, corresponds quite well to the one obtained in the physical measurement. Also the shape of the Energy-Collection Time correlation and its element dependence are quite well reproduced by the model. Nevertheless, the model still needs to be confronted with a broader collection of the experimental data obtained for detectors of various thicknesses and biased by various voltages.

Once tested on a broader collection of the experimental pulse shapes, the model will enable the theoretical search for the best identification method based on the pulse shape analysis. It will also enable the study of the dependence of the identification quality on the detector thickness and maybe on some special construction of the detector with non-linear electric field (obtained by the heterogeneity of doping) for regions with poor resolution (small ion energy, see Fig. 8). The presented approach should be also suitable for testing the temperature dependence (via the respective dependence of the diffusion coefficients).

In order to draw some more quantitative conclusions from the comparison of the model with the experimental data one has to estimate the uncertainties

related to various possible ingredients, mentioned in the previous paragraph. Also we have to make an attempt to constrain the single free parameter $\mu_{\sigma e}$ from the respective classical consideration.

The actual model calculation is quite time consuming. For standard processor the calculation of one pulse associated with the 80 MeV ^{12}C ion, takes about 5 hours of CPU, thus some code optimization is still needed.

Acknowledgment:

The author is indebted to J. Łukasik for careful reading of the manuscript and helpful discussions. Special thanks for H. Hamrita, for his calculations of the preamplifier response.

Work supported by Polish Ministry of Science and Higher Education under grant No. DPN/N108/GSI/2009

References

- [1] W. Seibt, et al., Nucl. Instr. and Meth. 113 (1973) 317.
- [2] P.A. Tove, W. Seibt, W. Leitz, Nucl. Instr. and Meth. 51 (1967) 304.
- [3] A.A. Quaranta, A. Taroni, G. Zanarini, IEEE Trans. Nucl. Sci. NS-15 (1968) 373.
- [4] H.O. Neidel, H. Henschel, Nucl. Instr. and Meth. 178 (1980) 137.
- [5] W. Bohne, et al., Nucl. Instr. and Meth. A 240 (1985) 145.
- [6] J.B. England, G.M. Field, T.R. Ophel, Nucl. Instr. and Meth. A 280 (1989) 291.
- [7] H. Hamrita, et al., Nucl. Instr. and Meth. A 531 (2004) 607.
- [8] M. Parlog, et al., Nucl. Instr. and Meth. A 613 (2010) 290.
- [9] J.F. Ziegler, et al., The Stopping and Range of Ions in Matter (SRIM), Pergamon Press, New York, 1985.
- [10] M. Papa et al., Phys. Rev. C 64 024612 2001

- [11] W. von Ammon, Nucl. Instr. and Meth. B 63 (1992) 95.
- [12] W.Shockley. Journ. Appl. Phys., vol.9, 635, (1938)
- [13] S. Ramo, Proc. I.R.E. 27 (1939) 584.
- [14] Hunsuk Kim, et al., Solid-State-Electronics, vol.34, no.11, 1251, (1991).

Figures

Figure 1. Allowing the charge induced by plasma in the detector electrodes. In the present approximation we consider only the nearest mirror reflections. So the influence of the charge induced in an electrode positioned at 0 on the detector electric field, acts as a part of the Gaussian localized in position $-x$ with the reverse charge and with the same variance. Similarly, the charge induced in the second electrode is represented by a respective Gaussian localized in a symmetric point at $2d_{Si} - x$.

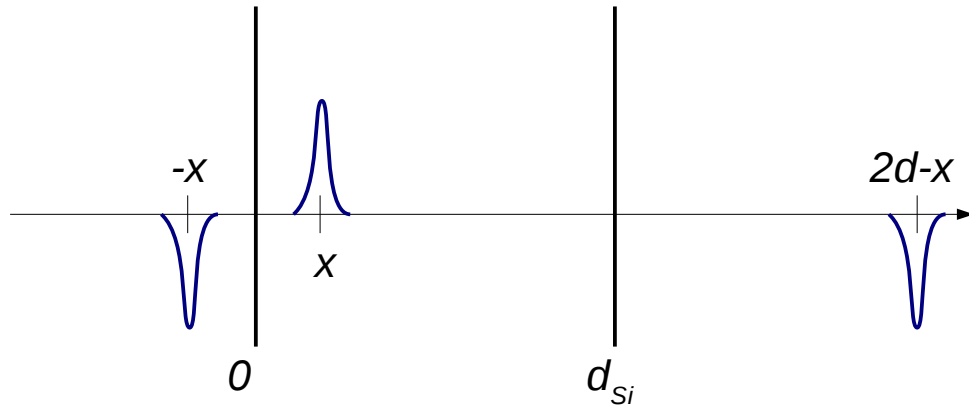


Figure 2. Propagation of the linear density of the electrons η_e (blue lines) and the holes η_h (red lines) due to the ionization induced by 80 MeV ^{12}C ion entering the Si detector from the rear side.

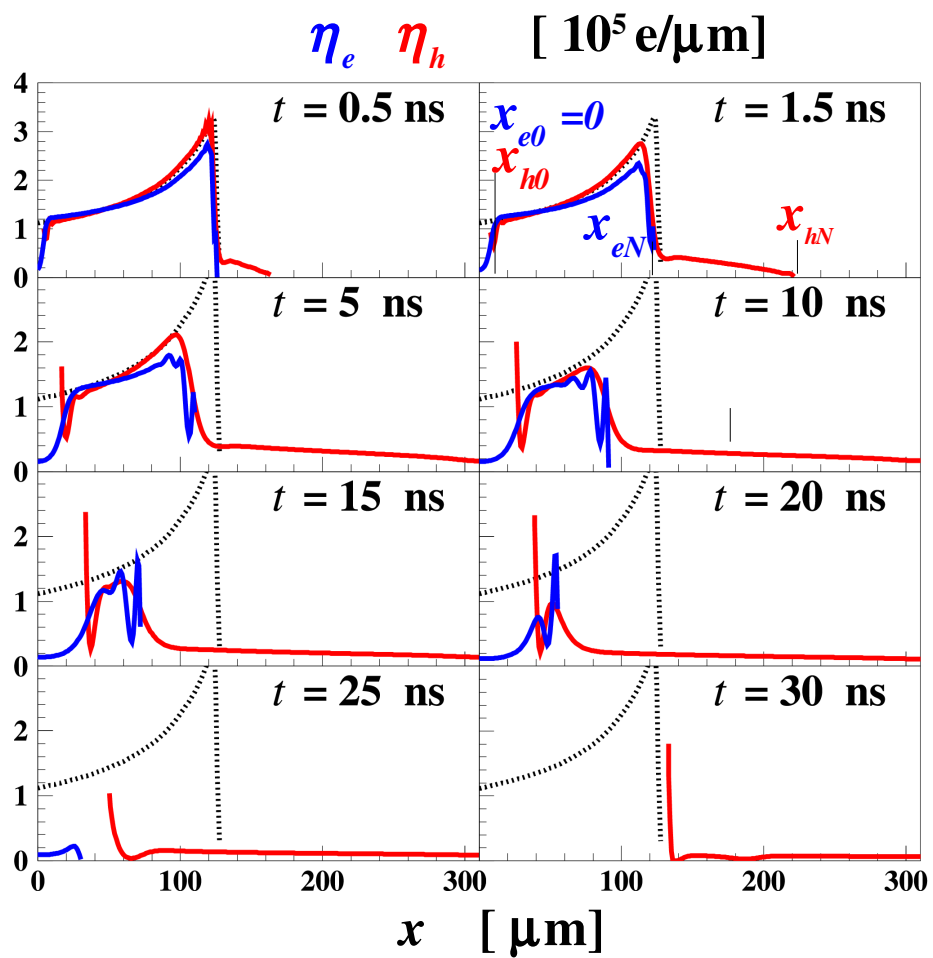


Figure 3. The effective electric field strength inside the silicon detector at different moments in time, due to the ionization induced by 80 MeV ^{12}C ion penetrating the detector from the rear side. The dotted line gives the undisturbed electric field for $t = 0$. The field is calculated only at points with coordinate x where the the density of electrons (blue line) and holes (red line) is not equal to zero.

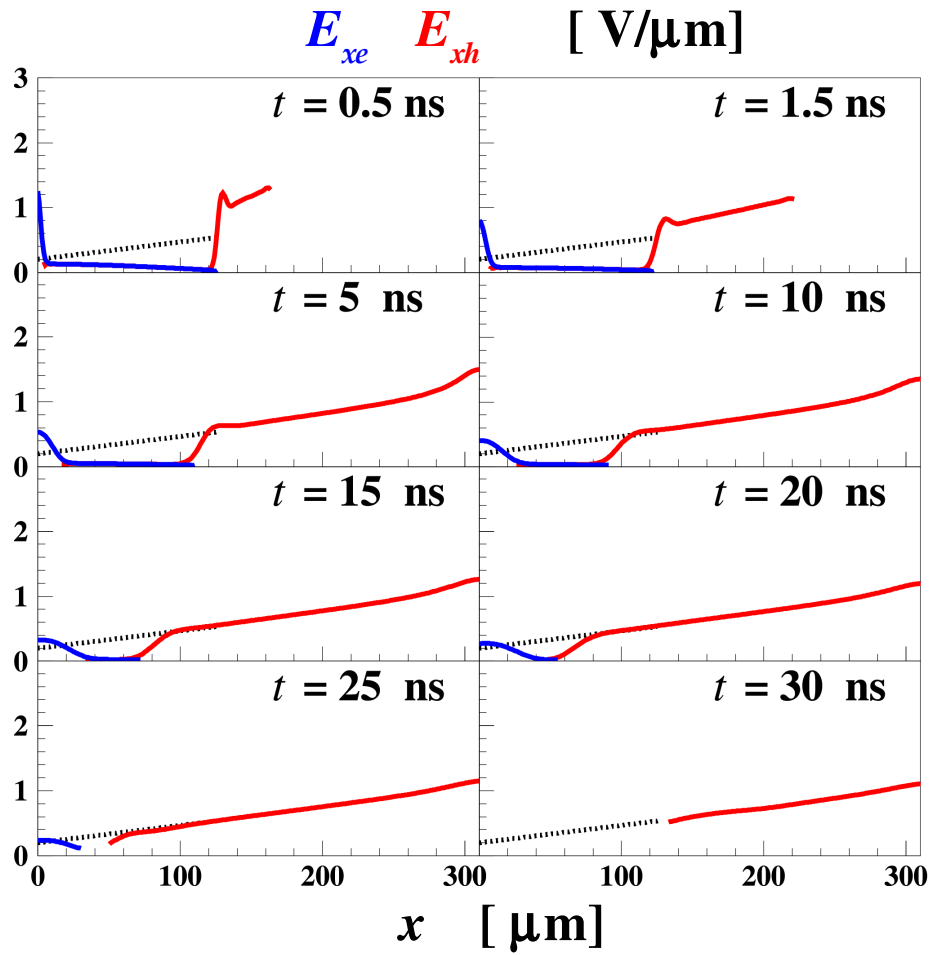


Figure 4. Time evolution of the width of the charge distribution which determines the charge propagation in the perpendicular direction. Standard deviations for electrons are represented by the blue line and variances for the holes by the red one.

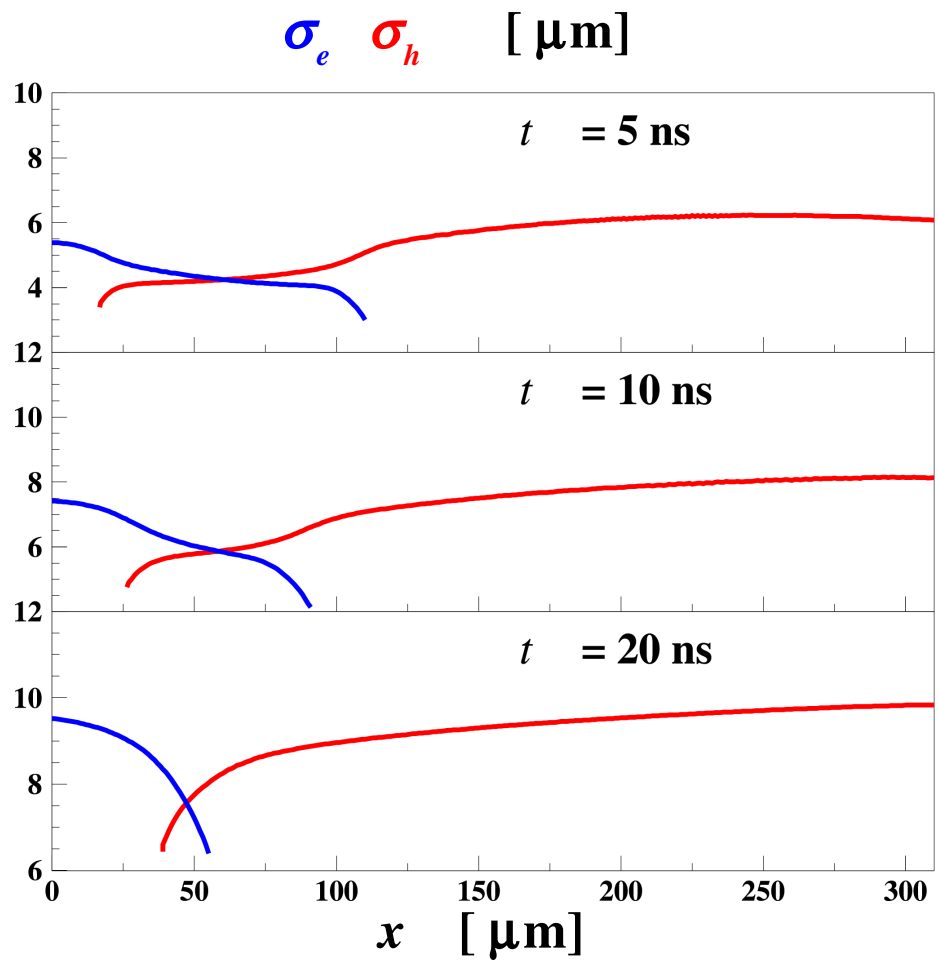


Figure 5. Same as Fig. 2, but neglecting the mutual Coulomb interactions between the carrier clouds. Significant difference in the charge collection time can be observed as compared to the complete case (see Fig. 2).

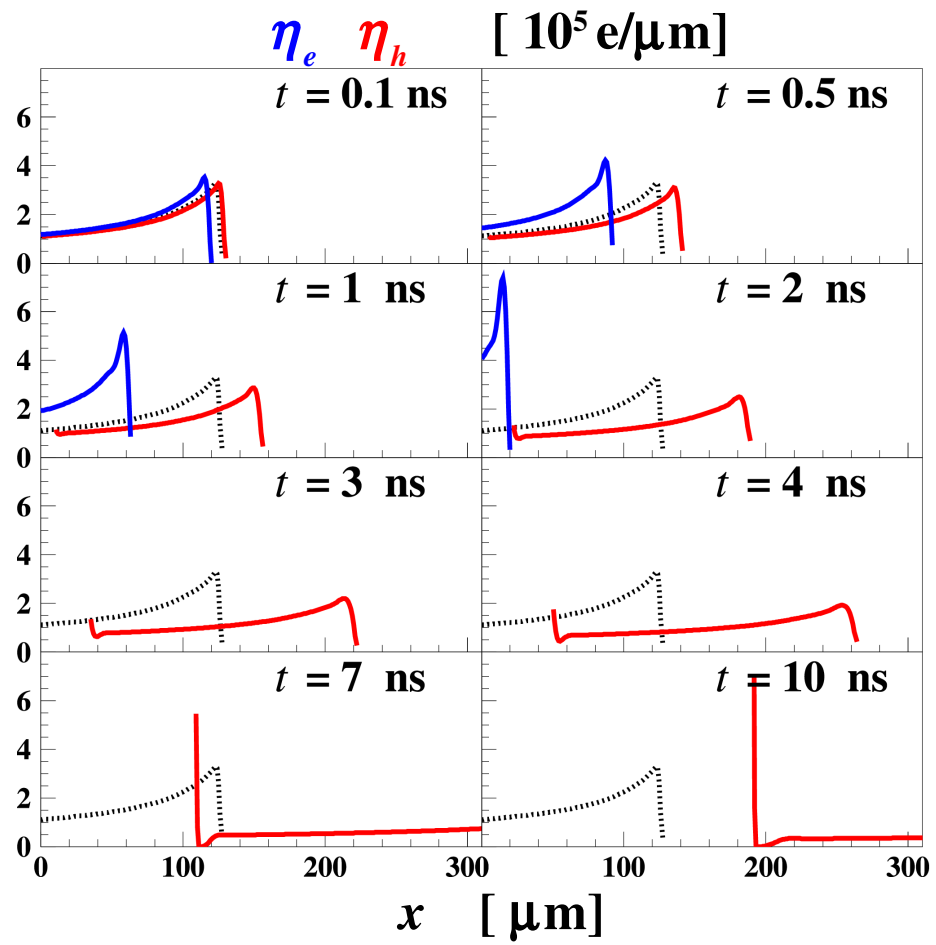


Figure 6. Model prediction of the current signal induced by an 80 MeV ^{12}C ion penetrating the silicon detector from the rear side. The predictions are not corrected for the preamplifier response. The solid, black line represents the total signal, the blue line presents the electron contribution while the red one the hole contribution. Mean experimental current signal is presented by the dashed line.

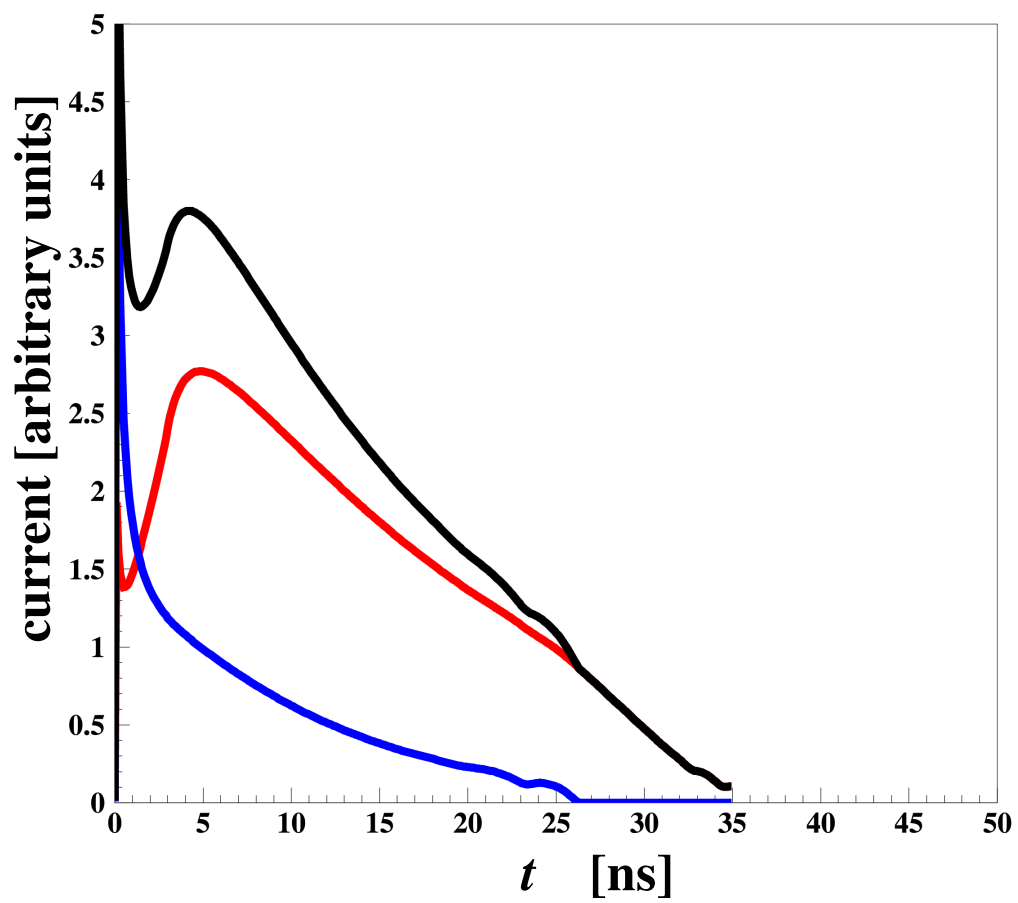


Figure 7. Same as Fig. 6 but the respective lines have been corrected for the preamplifier's response.

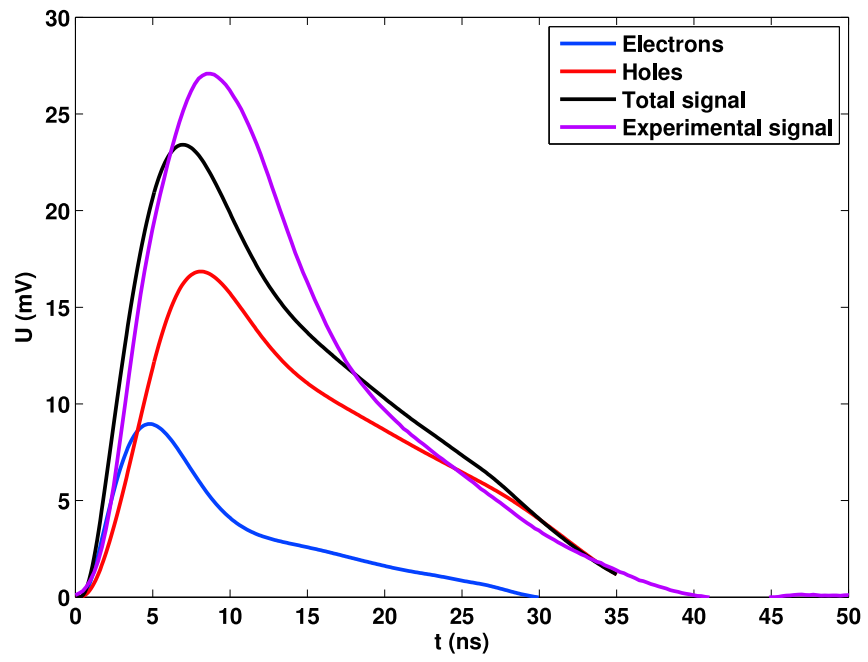


Figure 8. Model prediction for correlations: Energy vs Collection Time.

